View metadata, citation and similar papers at core.ac.uk
brought to you by CORE
provided by DSpace@MIT

The Astrophysical Journal, 690:440–452, 2009 January 1 doi:10.1088/0004-637X/690/1/440
© 2009. The American Astronomical Society. All rights reserved. Printed in the U.S.A.

THE X-RAY SPECTRUM OF A PLANETARY NEBULA AT HIGH RESOLUTION: *CHANDRA* GRATINGS SPECTROSCOPY OF BD +30°3639

Young Sam Yu[1], Raanan Nordon[2], Joel H. Kastner[1,3], John Houck[4], Ehud Behar[2,5], and Noam Soker[2]
[1] Center for Imaging Science, Rochester Institute of Technology, Rochester, NY 14623-5604, USA
[2] Department of Physics, Technion-Israel Institute of Technology, Haifa 32000, Israel
[3] Laboratoire d'Astrophysique de Grenoble, Université Joseph Fourier—CNRS, BP 53, 38041 Grenoble Cedex, France
[4] Kavli Institute, Massachusetts Institute of Technology, Cambridge, MA 02139, USA
Received 2008 June 13; accepted 2008 August 27; published 2008 December 1

ABSTRACT

We present the results of the first X-ray gratings spectroscopy observations of a planetary nebula (PN)—the X-ray-bright, young BD +30°3639. We observed BD +30°3639 for a total of ∼300 ks with the *Chandra X-ray Observatory's* Low Energy Transmission Gratings in combination with its Advanced CCD Imaging Spectrometer (LETG/ACIS-S). The LETG/ACIS-S spectrum of BD +30°3639 is dominated by H-like resonance lines of O VIII and C VI and the He-like triplet line complexes of Ne IX and O VII. Other H-like resonance lines, such as N VII, and lines of highly-ionized Fe are weak or absent. Continuum emission is evident over the range 6–18 Å. Spectral modeling indicates the presence of a range of plasma temperatures from $T_x \sim 1.7 \times 10^6$ K to 2.9×10^6 K and an intervening absorbing column $N_H \sim 2.4 \times 10^{21}$ cm^{-2}. The same modeling conclusively demonstrates that C and Ne are highly enhanced, with abundance ratios of C/O ∼ 15–45 and Ne/O ∼ 3.3–5.0 (90% confidence ranges, relative to the solar ratios), while N and Fe are depleted, with abundances N/O ∼ 0.0–1.0 and Fe/O ∼ 0.1–0.4, respectively. The intrinsic luminosity of the X-ray source determined from the modeling and the measured flux ($F_X = 4.1 \times 10^{-13}$ ergs cm^{-2} s^{-1}) is $L_X \sim 8.6 \times 10^{32}$ erg s^{-1} (assuming $D = 1.2$ kpc). These gratings spectroscopy results are generally consistent with earlier results obtained from X-ray CCD imaging spectroscopy of BD +30°3639, but are far more precise. Hence, the *Chandra*/LETG-S results for BD +30°3639 place severe new constraints on models of PN wind–wind interactions in which X-ray emitting gas within PNs is generated via shocks and the plasma temperature is moderated by effects such as heat conduction or rapid evolution of the fast wind. The tight constraints placed on the (nonsolar) abundances directly implicate the present-day central star—hence, ultimately, the intershell region of the progenitor asymptotic giant branch star—as the origin of the shocked plasma now emitting in X-rays.

Key words: planetary nebulae: general – planetary nebulae: individual (BD +30°3639) – stars: mass loss – stars: winds, outflows – stars: Wolf-Rayet – X-rays: ISM

Online-only material: color figures

1. INTRODUCTION

Planetary nebulae (PNs) are the last stages of evolution for intermediate-mass stars (1–8 $M_\odot$). The central star that generates a PN terminates its evolution as a cool asymptotic giant branch (AGB) star by ejecting its outer envelope. The ultraviolet (UV) radiation of the newly-exposed hot core—a future white dwarf (WD)—then illuminates and ionizes the ejected envelope. At about the same time, a "hot bubble" may be produced by collisions between the slowly expanding, ambient AGB gas and the newly-initiated fast central star wind (Kwok et al. 1978). Theories describing such wind interactions within PNs predict that the plasma temperature within the hot bubble should be high enough for the generation of soft ($\lesssim$ 1 keV) X-ray emission, and that the dimensions of the hot bubble X-ray source should be smaller than that of the optically emitting, ionized nebula (e.g., Zhekov & Perinotto 1996; Soker & Kastner 2003, and references therein). *ROSAT* X-ray observations of PNs appeared to offer early support for these predictions (Kreysing et al. 1992; Guerrero et al. 2000; however, also see Chu et al. 1993).

The advent of *Chandra* and *XMM-Newton* has provided far more convincing evidence of the presence of wind-blown hot bubbles within PNs (Kastner et al. 2008, and references therein; hereafter, K08). However, certain puzzling aspects of the wind-collision-generated hot bubbles within PNs remain to be explained. In particular, in contrast to the expectations of simple wind-collision models, the temperature of the X-ray emitting hot bubbles in PNs does not appear to depend on the present central star wind velocity (K08). Furthermore, the optical and X-ray emitting regions of the same object can display sharp differences in abundances (e.g., Maness et al. 2003, and references therein). These observations raise fundamental questions, such as: what heating and cooling mechanisms govern the temperature of the X-ray emitting plasma? Does the X-ray emission emanate primarily from the former AGB star wind, the present central star wind, or some mixture of the two?

BD +30°3639 ("Campbell's Star") is a young PN with a carbon-rich Wolf–Rayet ([WC]-type) central star; it has been studied at a wide variety of wavelengths (e.g., Li et al. 2002, and references therein). The nearby (distance ∼ 1.2 kpc; Li et al. 2002) BD +30°3639 has a young dynamical age (∼700 yr; Leuenhagen et al. 1996), and its fast wind speed is ∼ 700 km s^{-1} (Leuenhagen et al. 1996; Marcolino et al. 2007). It is an excellent target for X-ray observations, due to its unusually large soft X-ray flux at earth ($F_X \sim 4 \times 10^{-13}$ erg cm^{-2} s^{-1}, 0.1–2.0 keV; Kreysing et al. 1992; Arnaud et al. 1996). Kreysing et al. (1992) first detected X-rays from BD +30°3639 with *ROSAT* and estimated the hydrogen column density toward and plasma

[5] Senior NPP Fellow, Code 662, NASA/Goddard Space Flight Center, Greenbelt, MD 20771, USA.

Table 1
Chandra Observations of BD +30°3639

Obs. ID	Date	Instrument	Exposure (ks)	Zeroth-Order (Counts) Source (Background)	First-Order (Counts) Source (Background)
587	2000 Mar 21	ACIS-S3	18.8	4762 (238)	N/A
5409	2006 Feb 13	LETG/ACIS-S	85.4	2039 (964)	1742 (764)
7278	2006 Mar 22	LETG/ACIS-S	61.8	1441 (655)	1231 (593)
5410	2006 Dec 20	LETG/ACIS-S	53.9	1187 (572)	1043 (495)
8495	2006 Dec 21	LETG/ACIS-S	77.1	1713 (821)	1480 (763)
8498	2006 Dec 24	LETG/ACIS-S	19.9	511 (214)	386 (211)

Note. Source counts are calculated without subtracting background.

temperature within the X-ray nebula ($N_H \sim 1.4 \times 10^{21}$ cm^{-2} and $T_x \sim 2.5 \times 10^6$ K, respectively). The latter result ruled out, for example, a hot companion to the ∼30 kK central star as the X-ray source and suggested the presence of a wind-shock-generated hot bubble within BD +30°3639.

Using the *Chandra* Advanced CCD Imaging Spectrometer (ACIS), Kastner et al. (2000) demonstrated that X-ray emission from BD +30°3639 was spatially extended and that the X-ray emitting gas was fully confined within the ∼5″ diameter elliptical ring of photoionized gas seen in optical and IR images. While these results supported the existence of a "classical" hot bubble within BD +30°3639, one could not rule out other possibilities, such as jets resulting from binary interactions (Bachiller et al. 2000; Kastner et al. 2001, 2002; Soker & Kastner 2003; Akashi et al. 2008). Whether the X-ray emitting gas comes from jets or a fast spherical wind, there remains the question of the role, if any, of heat conduction between the X-ray emitting gas and the visible shell (Soker 1994; Zhekov & Perinotto 1996; Zhekov & Myasnikov 1998, 2000), and/or mixing of the two media (Chu et al. 1997) enhanced by instabilities (Steffen et al. 2005, 2008; Stute & Sahai 2006; Schönberner et al. 2006), in moderating the X-ray temperature to levels well below those expected from collisions between the present-day 700 km s^{-1} stellar wind and the previously-ejected AGB star envelope.

The source of the X-ray emitting gas in BD +30°3639 also remains to be determined, even though it has been a favorite subject of X-ray CCD spectroscopy. Arnaud et al. (1996) obtained estimates of X-ray plasma abundances using *ASCA* CCD imaging spectrometer data, finding C, N, and Ne to be significantly overabundant and Fe to be significantly depleted. Similar results were obtained via analysis of *Chandra* and Suzaku CCD imaging spectroscopy (Kastner et al. 2000; Maness et al. 2003; Murashima et al. 2006). However, these results are somewhat at odds with those obtained from optical/IR wavelengths that show, for example, depleted Ne in the bright shell of the PN. While the presence of an enhanced Ne abundance in the X-ray emitting plasma seems reasonably secure, the degree of Ne overabundance and other abundance anomalies—such as highly enhanced C and highly depleted Fe, also inferred on the basis of X-ray CCD spectral modeling—remain quite uncertain. Indeed, Georgiev et al. (2006) argued that X-ray CCD spectra cannot provide definitive constraints on the plasma abundances in PNs.

To make progress on these and other problems concerning the nature and origin of the X-ray emitting plasma within PNs requires X-ray observations at high spectral resolution, from which we unambiguously infer, with improved precision, the temperature and composition of the X-ray emitting plasma. With this motivation, we obtained a deep observation of BD +30°3639 using *Chandra*'s Low Energy Transmission Gratings spectrometer in combination with its Advanced CCD Imaging Spectrometer (LETG/ACIS-S). We selected LETG/ACIS-S (as opposed to high energy (HE) TG/ACIS-S or LETG/high resolution camera (HRC)-S) for *Chandra* grating observations of BD +30°3639 on the basis of the superior background rejection, soft X-ray sensitivity, and order-sorting capabilities of this configuration. In addition to the dispersed spectrum of BD +30°3639 (for which preliminary results were presented in Kastner et al. 2006), the LETG/ACIS-S observations produced a highly-sensitive, undispersed zeroth-order image of the PN. In this paper, we present a comprehensive analysis of the dispersed LETG/ACIS-S spectrum of BD +30°3639. In a subsequent paper (Y. S. Yu et al. 2008, in preparation), we present a spatial/spectral analysis of the LETG/ACIS-S zeroth-order image of BD +30°3639 and compare this image with the direct *Chandra*/ACIS-S3 image obtained in Cycle 1 observations.

2. OBSERVATIONS AND DATA REDUCTION

We obtained observations of BD +30°3639 totaling nearly 300 ks exposure time with LETG/ACIS-S in 2006 February (85.4 ks), March (61.8 ks), and December (150.9 ks). The last observation was obtained in three consecutive blocks at the same roll angle. The event data were subject to standard pipeline processing (using *Chandra* X-ray Center pipeline versions 7.6.7 for the 2006 February and March data and 7.6.9 for the 2006 December data). In Table 1, we list exposure times and total photon counts within the source and background regions. To determine total counts in the zeroth-order images, we selected a 10″ circular region centered on the source and a surrounding annular region (with inner and outer radii of 13″ and 20″, respectively) for the background. The total first-order counts were directly determined from the extracted source and background spectra (Section 3). We also extracted light curves from the source regions of the 2000 image and the zeroth-order images obtained in 2006; no measurable variability was found, as expected, given the diffuse nature of the source.

Because the first two observations in 2006 (observation IDs (ObsIDs) 5409 and 7278) were obtained at different spacecraft roll angles and aimpoints with respect to each other and the last three (December) 2006 observations, we cannot generate a merged spectral image for the full 300 ks exposure. However, the second (December 2006) half of the 300 ks exposure (ObsIDs 5410, 8495, and 8498) was obtained at a constant roll angle, so we generated a single, 150 ks exposure dispersed spectral image from these data by merging the three Level 2 event (`evt2`) files. The full spectral images obtained from the resulting combined `evt2` files are shown in Figures 1 and 2. These dispersed images demonstrate that the LETG/ACIS-S X-ray counts spectrum of BD +30°3639 is dominated by emission lines of highly ionized (He-like and H-like) ions of oxygen and neon.

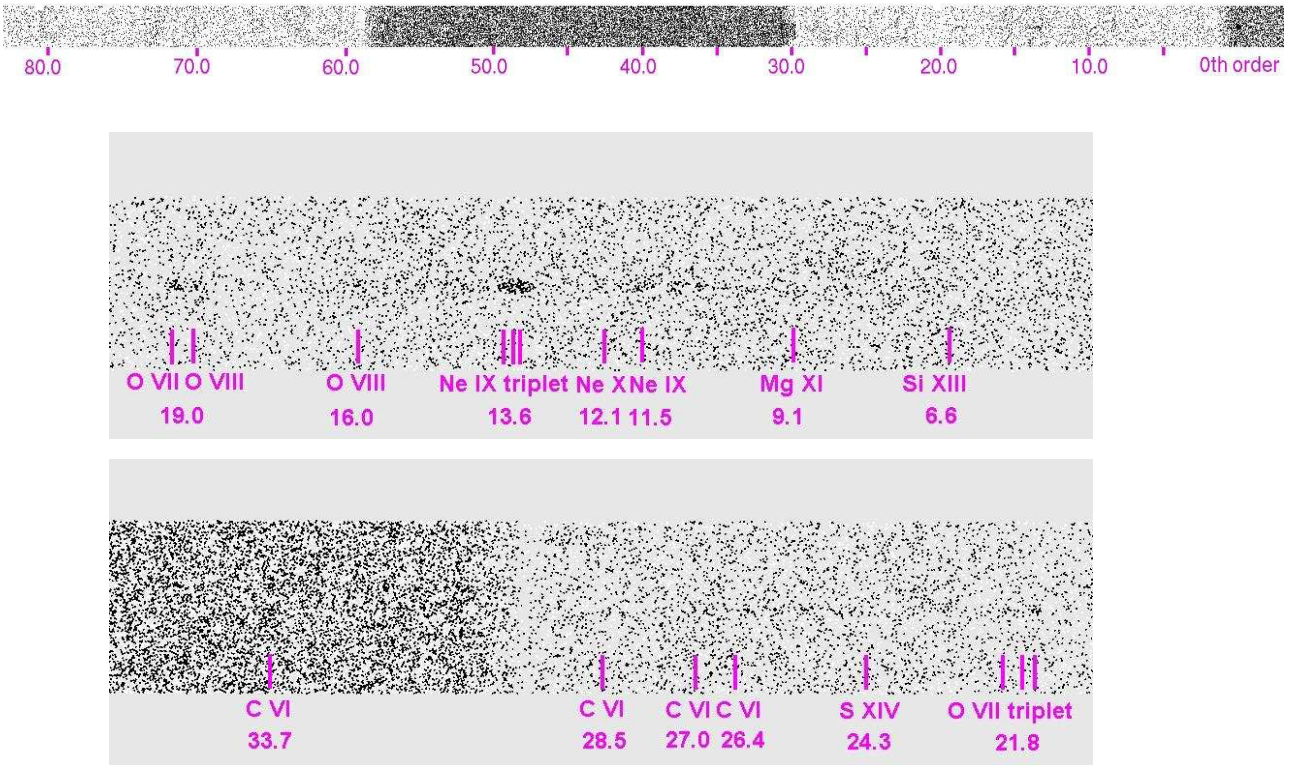

Figure 1. Dispersed spectral images of BD +30°3639 for negative LETG orders, with wavelength scales (in Å) overlaid. Top: full range of negative orders. Middle and bottom: closeups of dispersed spectral images over the wavelength ranges 5–20 Å and 20–35 Å, respectively.
(A color version of this figure is available in the online journal.)

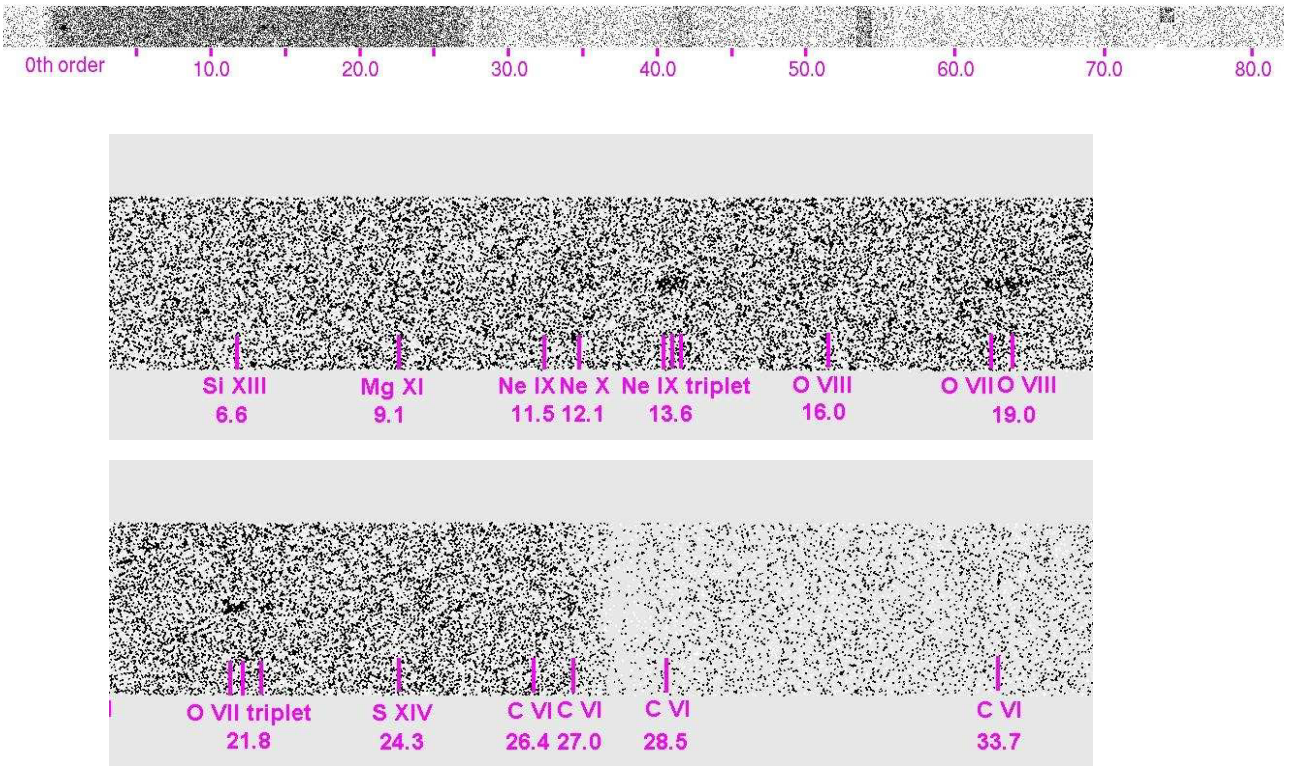

Figure 2. As in Figure 1, for positive LETG orders.
(A color version of this figure is available in the online journal.)

For analysis of the dispersed spectrum, further processing involved removal of artifacts on ACIS-S4 (using the Chandra Interactive Analysis of Observations (CIAO) tool "destreak") and applying updated calibrations. Standard gratings point-source spectral extraction threads available in CIAO[6] were used to generate spectrum pulse height amplitude (PHA) files and corresponding redistribution matrix files (RMFs) and auxiliary response files (ARFs). These threads implicitly ignore the (non-negligible, ∼5″) spatial extension of the BD +30°3639 X-ray source, resulting in artificially "broadened" emission line features (we discuss this effect further in Sections 3.1 and 3.2). We extracted positive ($m = +1$) and negative ($m = -1$) first-order LETG spectra for each of the five observations (Table 1). To enhance the signal-to-noise ratio, each LETG spectrum was rebinned by a factor of 8, resulting in a wavelength dispersion of 0.1 Å/bin. We then merged the resulting spectra into a single spectrum. In parallel, the corresponding ARFs were averaged and weighted by the relative exposure times and then merged into a single ARF. The various RMFs obtained from the individual observations for a given order are identical to within the calibration uncertainties. Hence, for the spectral analysis described below, we used the same, representative RMF for each LETG dispersion arm.

3. ANALYSIS AND RESULTS

The merged, 300 ks exposure time spectrum resulting from the LETG/ACIS spectral image data reduction procedure described in Section 2 is displayed in Figure 3(a). The spectrum displays strong emission lines superposed on a weak continuum, with an abrupt rise in the continuum at ∼30 Å that is likely due to background events. To account for this apparent residual background, we identified a region devoid of bright X-ray sources, displaced 215 arcsec from the source position along the detector *y* direction, and extracted first-order background spectra at this position from each of the five observations. The corresponding RMFs and ARFs of background spectra were also generated. We rebinned and merged these individual background spectra into a single spectrum (seen superimposed on the source spectrum in Figure 3(a)). Figure 3(b) shows the resulting combined, first-order, background-subtracted spectrum of BD +30°3639 in the wavelength range of 5–40 Å. The apparent "continuum" in the region 30–40 Å is effectively removed from this background-subtracted spectrum.

The brightest lines in the background-subtracted spectrum of BD +30°3639 are due to highly ionized (H- and He-like) species of C, O, and Ne; the resonance lines of H-like O VIII (λ18.97) and C VI (λ33.6) and the He-like triplet line complexes of Ne IX (λ13.45, 13.55, 13.7) and O VII (λ21.60, 21.80, 22.10) are especially prominent. Other H-like resonance lines, such as N VII (λ24.78), and lines of highly ionized Fe are weak or absent. Continuum emission is evident over the range 6–18 Å. The excess emission near 25 Å can likely be attributed to enhanced high-order lines of C VI within its H-like recombination line spectrum (R. Nordon et al. 2008, in preparation).

3.1. Line Identifications, Fluxes, and Source Angular Sizes

We measured line fluxes with the Interactive Spectral Interpretation System (ISIS[7]; Houck & Denicola 2000). Given the relatively symmetric appearances of the profiles of prominent emission lines, we used a fit function consisting of a constant local continuum (polynomial) plus one or more Gaussian functions. In fitting the strong He-like triplet lines (Ne IX and O VII), the ratios of line strengths and widths of the triplet components were fixed using the values given by the *Chandra* atomic database (ATOMDB ver. 1.3) for the case of low-density plasma ($n_e \ll 10^{10}$ cm^{-3}). Thus, the free parameters were the intensities of triplets, the line-center wavelength and full width at half-maximum (FWHM) of one of the triplets, and the coefficients of the polynomial representing the local continuum.

For those emission lines that could be measured with acceptable statistics, Table 2 lists the line identifications, fluxes, and widths. The line-fitting procedure thereby confirms the identification of at least 15 lines and line complexes in the LETG spectrum of BD +30°3639, ranging from the very strong C VI Lα line to weak Mg XII and Si XIII lines. The table also lists upper limits on the fluxes of the lines of other ions that are of ionization potential similar to the well-detected species such as Ne IX, Ne X, O VII, O VIII, and C VI. Lines of these important species—for example, Fe XVII and N VII—should be prominent in the spectrum of a solar-abundance plasma at the approximate temperature implied by the well-detected lines ($T_x \sim 2 \times 10^6$ K).

Since the X-ray line widths reflect the extended nature of the source rather than, for example, plasma turbulence (see below) or kinematics, the width measurements for well-detected lines (Δλ) are expressed in terms of the corresponding angular FWHM in arcsec, assuming a dispersion for LETG of 18.02 arcsec Å^{-1} (Dewey 2002). The resulting angular FWHMs are consistent with each other and with the (∼5″) source angular extent in the zeroth-order image, within the uncertainties. Furthermore, there are no discernible systematic redshifts or blueshifts measured for the emission line centers. Hence, for purposes of the plasma modeling described here, all of the emission lines can be considered to arise from the same region within the nebula.

3.2. Global Spectral Fitting

Global X-ray spectral model fitting of lines and underlying continuum is necessary to simultaneously constrain relative plasma elemental abundances and temperatures. In adopting this approach to fit the LETG spectrum of BD +30°3639, we selected the "*Cash*" method (Cash 1979) as the fit statistic to treat low count data. For the model fitting, we specified the displaced background spectrum (see Section 3.1) along with the merged source spectrum. To investigate plasma physical conditions, we used ISIS to construct Astrophysical Plasma Emission Database (APED; Smith et al. 2001) models, varying plasma metal abundances, such as Fe, Ne, O, C, N, and Mg, and leaving all other abundances, including H and He, fixed at solar (Anders & Grevesse 1989). The latter assumption is, of course, unlikely to be valid if the X-ray-emitting plasma is dominated by the H-depleted, He-enriched wind characteristic of the present-day central star (e.g., Marcolino et al. 2007)—a hypothesis that is indeed supported by our modeling results (see Sections 3.2.2 and 4.1). We did not consider higher Lyman series C VI lines that lie in the region ∼25–29 Å in the spectral model because the APED only includes the C VI Lyman series up to the δ line. Analysis of these higher-energy C VI transitions is described in R. Nordon et al. (2008, in preparation).

[6] http://cxc.harvard.edu/ciao/threads/spectra_letgacis/
[7] http://space.mit.edu/CXC/ISIS/

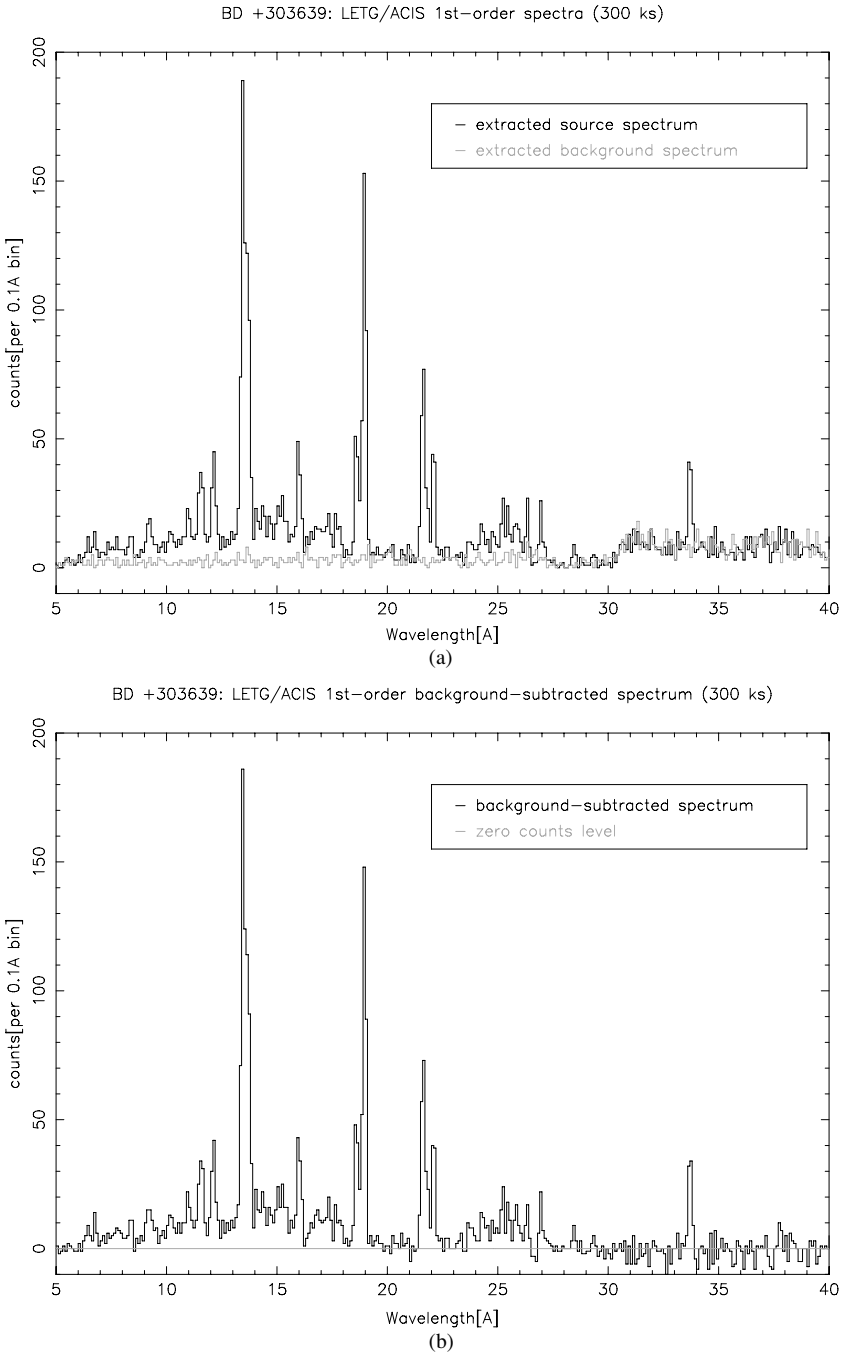

Figure 3. (a) Combined positive and negative first-order LETG/ACIS-S counts spectra of BD +30°3639 (black) and background (gray). (b) Background-subtraction counts spectrum of BD +30°3639.

3.2.1. Isothermal Versus Two-Component APED Models

To reproduce the merged LETG first-order spectrum of BD +30°3639, we attempted fits with both single-component and two-component APED plasma models. Note that the spectral resolving power of LETG for a point source ranges from $E/\triangle E \sim 130$ at 5 Å to $E/\triangle E \sim 1000$ at 40 Å (Dewey 2002). The spatial extension of BD +30°3639 (FWHM ∼ 3 arcsec; Table 2), combined with use of ACIS-S rather than HRC as the detector, then degrades the effective resolving power of LETG by a factor of ∼3 (Dewey 2002). Source spatial extent—rather than, for example, gas turbulence or thermal broadening—therefore determines the line widths. To emulate this artificial line "broadening," we used the turbulent velocity parameter ($V_{\rm turb}$) available in the APED model. We find that two turbulent velocity components—with best-fit parameter values of ∼1700 km s^{-1} and ∼900 km s^{-1} for the short- and long-wavelength spectral regions, respectively, consistent with the mean FWHM measured for the lines—are sufficient to reproduce the "broadening" caused by the extended X-ray source within BD +30°3639. We emphasize that these results do not actually represent measurements of gas turbulence; rather, like emission line FWHM (Table 2), the best-fit $V_{\rm turb}$ values serve as an indication of source spatial extent.

Each of the models was assumed to undergo absorption due to intervening neutral material characterized in terms of the

Table 2
List of Line Fluxes of BD +30°3639

Line	λ_{lab}[a] (Å)	λ_o[b] (Å)	FWHM[c] (arcsec)	f_l[d] (10^{-6} photons cm^{-2} s^{-1})
Si XIII	6.648	6.781	...	0.27 [0.06–1.42]
Mg XII	8.419	8.401	...	0.5 [0.1–1.0]
Mg XI	9.169	9.203	4.6 [1.1–20.1]	1.1 [...]
	9.231	9.265	"	1.2e-4 [...]
	9.314	9.348	"	0.4 [...]
Ne IX	11.544	11.563	3.9 [2.3–5.8]	4.8 [2.8–7.4]
Ne X	12.132	12.126	2.5 [0.001–3.9]	3.8 [2.3–5.7]
Ne IX	13.447	13.457	2.9 [2.4–3.4]	27.2 [21.6–33.2]
	13.553	13.563	"	6.2 [0.7–11.2]
	13.699	13.709	"	16.7 [13.4–20.1]
Fe XVII	15.014	...	...	(2.0)[e]
O VIII	15.176	15.191	...	6.3 [1.8–18.0]
O VIII	16.004	15.997	...	5.2 [2.7–14.5]
Fe XVII	16.780	...	...	(0.5)[e]
Fe XVII	17.051	...	...	(0.3)[e]
Fe XVII	17.096	...	...	(0.2)[e]
O VII	18.627	18.618	3.8 [2.5–5.0]	17.9 [13.0–22.1]
O VIII	18.967	18.966	2.5 [2.1–3.0]	40.0 [34.0–46.0]
O VII	21.602	21.607	2.8 [2.2–3.3]	38.2 [31.1–44.8]
	21.807	21.809	"	13.1 [7.8–17.8]
	22.098	22.103	"	27.7 [21.1–34.0]
S XIV	24.285	24.322	...	5.1 [0.5–21.8]
N VII	24.7798	...	...	(9.0)[e]
C VI	26.357	26.330	2.4 [1.5–3.5]	11.2 [4.9–17.3]
	26.990	26.963	"	22.9 [13.1–33.0]
	28.465	28.438	"	31.4 [10.0–53.5]
C VI	33.734	33.708	2.7 [1.3–4.0]	98.0 [79.0–145.0]
C V	34.973	...	...	(25.0)[e]

Notes.
[a] Theoretical wavelength of identification, from APED. In case of a multiplet, we give the wavelength of the stronger component.
[b] Measured wavelength.
[c] FWHM of emission lines in units of arcsec; see Section 3.1.
[d] Line flux; 90% confidence intervals are given in brackets.
[e] Flux is a 2σ upper limit. The line detected at 15.1911 Å line may be a blend of λ15.176 O VIII and λ15.014 Fe XVII, but we estimate that the Fe XVII line contributes no more than ∼50% of the blended line flux.

column density of neutral H, $N_{\rm H}$, using the standard, solar-abundance (`wabs`) model (Morrison & McCammon 1983). However, note that, given the close correspondence between the visual extinction and X-ray surface brightness distributions of BD +30°3639 (Kastner et al. 2002), the absorption is, in fact, best attributed to the nebula itself rather than intervening interstellar medium (ISM). The X-ray-absorbing material may be the extended molecular envelope of BD +30°3639, pockets of cold, dense gas embedded in the ionized nebula, or some combination of these contributions; as a result, the composition of the absorbing material may differ significantly from that assumed in the `wabs` model. The implications for the results for $N_{\rm H}$, as well as for model plasma abundances, are discussed below.

Figure 4(a) shows the merged, 300 ks exposure, first-order LETG/ACIS-S counts spectrum of BD +30°3639, overlaid with the single-component model spectrum obtained from the APED. The comparison of the flux-calibrated spectrum with the model makes apparent the strength of C VI (λ33.6) relative to the other strong lines (Ne IX, O VII, and O VIII; Figure 4b). Other features apparent in the long wavelength (λ > 30 Å) region of the flux-calibrated spectrum are likely artifacts of poor photon counting statistics combined with the very low net effective area of LETG/ACIS in this region. However, we find that this single-component APED model is insufficient to adequately fit the spectrum. In particular, while the O VII to O VIII line ratios are reasonably well reproduced, the model cannot simultaneously fit the Ne IX and Ne X lines in the 12 Å region.

In contrast, the two-component APED model well reproduces the intensities of all strong emission lines and better matches the 6–18 Å continuum (Figure 5). The high-temperature boundary is constrained in part by the nondetection of the Mg XII line at 8.42 Å contrasted with the weak but clear Mg XI line at 9.12 Å. The low-temperature boundary is harder to constrain, as it relies, in part, on the relative intensities of the (somewhat noisy) C VI lines at 28.46 Å and 33.73 Å. Since the plasma temperatures are, therefore, mainly governed by two indicators—that is, the line ratios of the H-like to He-like O and Ne—introducing more than two temperature components into the model would make the fit result degenerate.

3.2.2. Best-Fit Parameters: Results and Confidence Ranges

The best-fit temperature of the single-component APED model indicates that, under the isothermal plasma approximation, the characteristic plasma temperature lies in the range 2.2–2.4 × 10^6 K. It is, therefore, not surprising that the values of T_X obtained from the two-temperature-component model

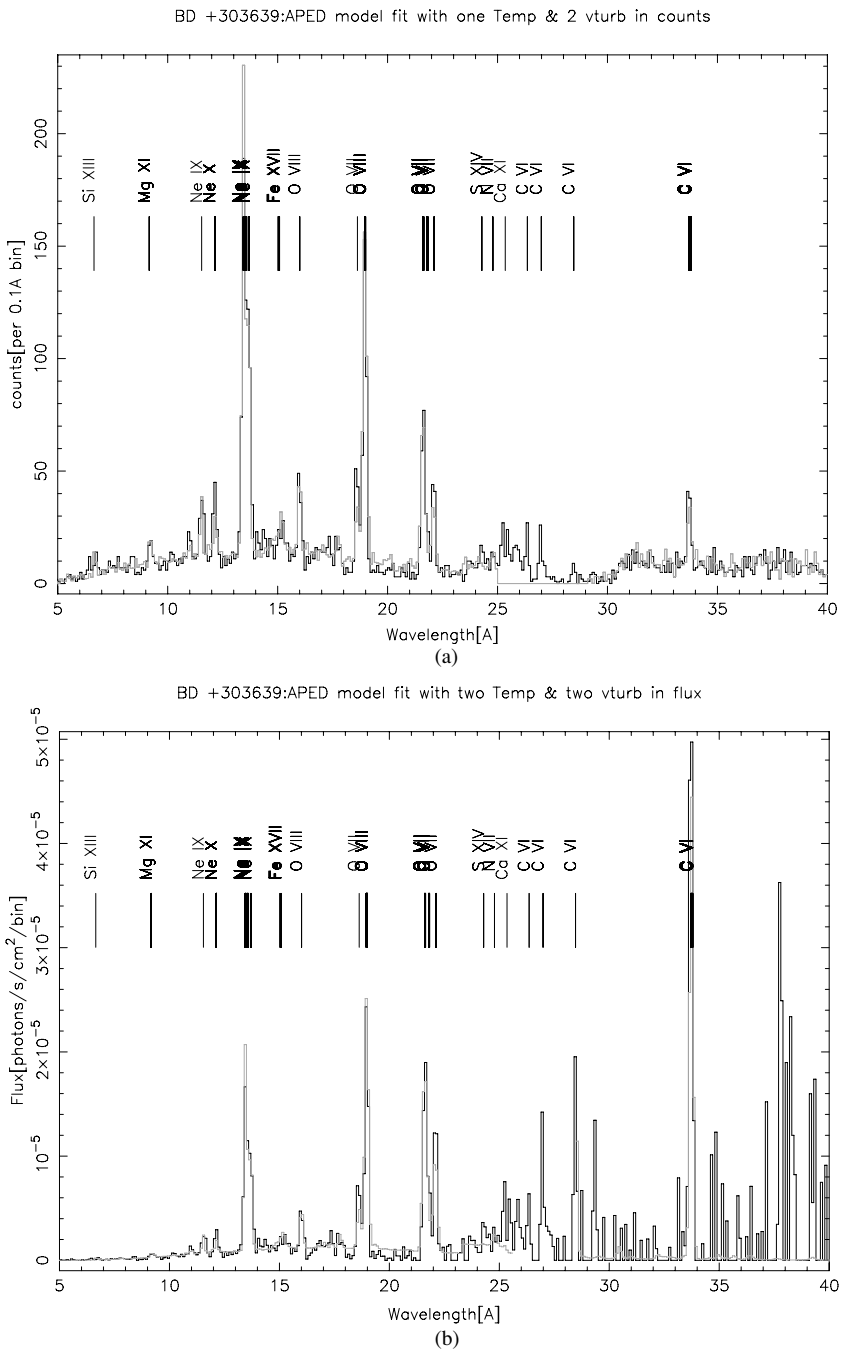

Figure 4. (a) Combined positive and negative first-order LETG/ACIS-S counts spectrum of BD +30°3639 (including background) overlaid with the best-fit single-component APED model. (b) Flux-calibrated first-order LETG/ACIS-S spectrum, overlaid with the same model. In each panel, black shows the source spectrum and gray indicates the model.

($T_1 = 2.9 \times 10^6$ K and $T_2 = 1.7 \times 10^6$ K) bracket this range. Table 3 demonstrates that the two preceding models also yield consistent results where plasma abundances are concerned but that the two-component model, in addition to providing a superior fit to the LETG spectrum, yields these abundance results to greater precision.

We reiterate that the best-fit absolute abundances listed in Table 3 (as number ratios relative to solar) were obtained under the assumption of solar H and He abundance (Anders & Grevesse 1989) and are, therefore, subject to large but unknown systematic uncertainties. Specifically, no diagnostics of H and He abundances are available in the X-ray regime, yet it is likely that the X-ray emitting plasma is dominated by present-day (H-depleted, He-enriched) [WC] stellar wind material (Section 4.1). In this case of a strongly H-depleted stellar wind, the abundance normalization to H becomes irrelevant. One could, however, renormalize the Table 3 results to the solar He abundance under the assumption that ratio of the C-to-He abundances is identical to the [WC] stellar wind value, that is, C/He ~ 0.4 by number (Marcolino et al. 2007) or ~ 108 times the solar ratio. The values listed in Table 3 could then be increased by a factor $108/28.3 = 3.8$, where 28.3 is the C abundance obtained from the two-component model fit, so as to yield elemental abundances relative to He in solar units. The results for emission

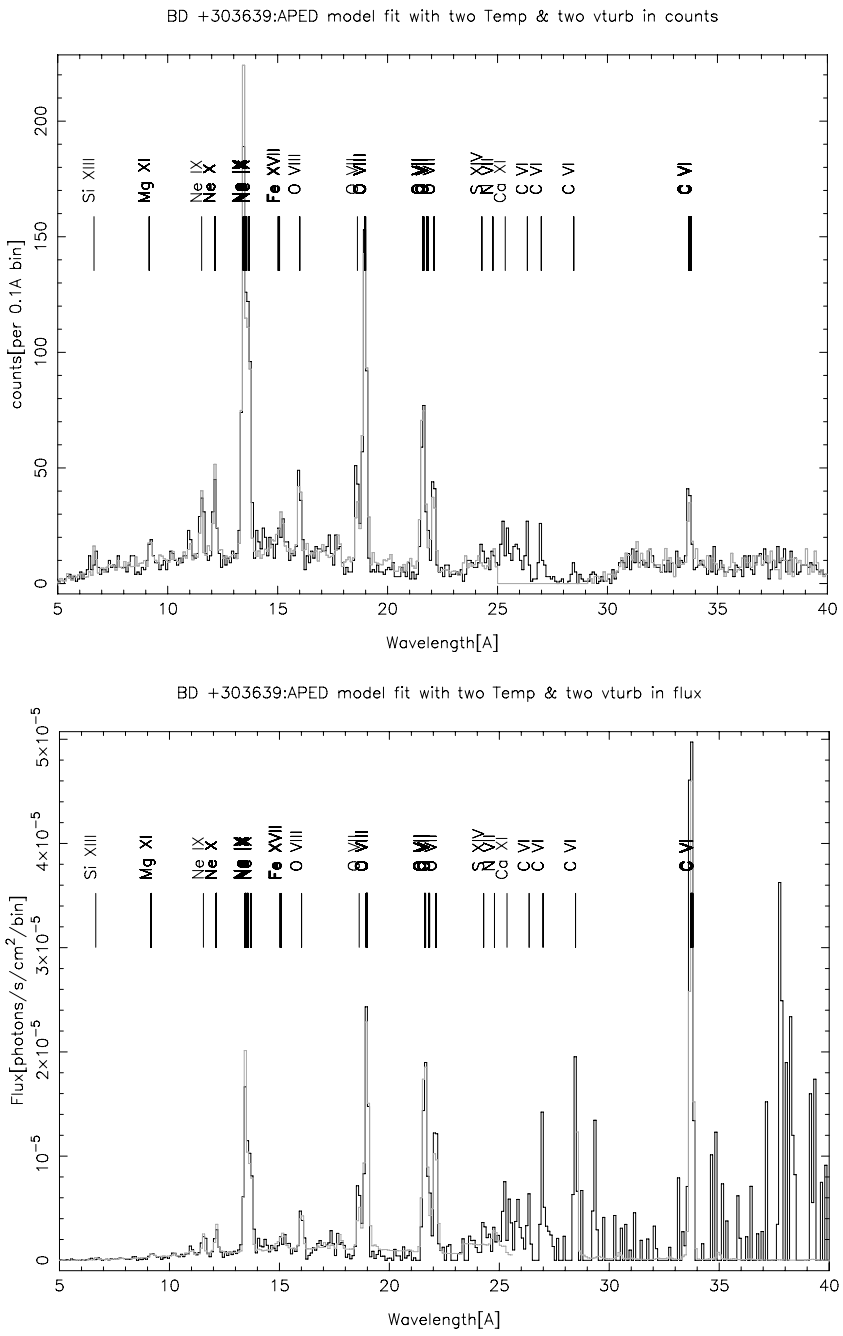

Figure 5. As in Figure 4, but for the best-fit two-component APED model.

measure would then also have to be redefined to refer to the number density of He nuclei (rather than H). In the context of the APED model, this is equivalent to reducing the model normalization by the same factor as that of the increase in elemental abundances.

Given the foregoing problems in attempts to determine absolute abundances, all subsequent analysis in this paper is based on the modeling results for abundances as number ratios relative to O. In this regard, the results listed in Table 3 then indicate that C is very overabundant (C/O $\sim$ 30, relative to the solar ratio), Ne is overabundant (Ne/O $\sim$ 3.8), and both Fe and N are likely depleted (Fe/O $\sim$ 0.2 and N/O $\sim$ 0.4).

Because the LETG response matrix is nearly diagonal, the observed (absorbed) source X-ray flux deduced from the model fitting is similar for the two models ($F_X = 4.4 \times 10^{-13}$ erg cm^{-2} s^{-1}). The inferred intrinsic (unabsorbed) X-ray source luminosity is then constrained by the model fitting to lie in the range from 7.4×10^{32} erg s^{-1} to 8.6×10^{32} erg s^{-1}. The low-T and high-T components of the latter model account for $\sim$25% and $\sim$75% of the total source luminosity, respectively.

In Figures 6–8, we present plots of confidence contours obtained from the two-component APED model for various parameter combinations. Figure 6 demonstrates that $N_{\rm H}$, which is mainly constrained by the relative strengths of metal lines in the softer part of spectrum, is (in principle) very well determined, and that this parameter is essentially insensitive to the plasma temperature and C and O abundances obtained from the model fitting. Given a standard (ISM) gas-to-dust (hence, $N_{\rm H}/A_{\rm V}$) ratio, the best-fit value of $N_{\rm H} = 2.4 \times 10^{21}$ cm^{-2} obtained from the two-component model is roughly consistent

Table 3
BD +30°3639: APED Model Fitting Results[a]

Parameter	Single-Component APED Model	Two-Component APED Model
N_H (10^{22} cm^{-2})	0.21 [0.19–0.24]	0.24 [0.20–0.28]
EM$_1$[b]	2.8×10^{55} [(2.1–4.0) $\times 10^{55}$]	6.9×10^{54} [(3.4–13.8) $\times 10^{54}$]
EM$_2$[b]	...	1.7×10^{55} [(1.0–2.2) $\times 10^{55}$]
T_1 (10^6 K)	2.3 [2.2–2.4]	2.9 [2.6–3.3]
T_2 (10^6 K)	...	1.7 [1.3–2.1]
C	19.50 [12.29–28.82]	28.30 [16.05–45.85]
N	0.17 [0.02–0.39]	0.38 [0.08–0.87]
O	0.44 [0.26–0.67]	0.87 [0.57–1.29]
Ne	2.03 [1.39–2.85]	3.30 [2.21–4.16]
Mg	0.60 [0.23–0.97]	0.63 [0.31–1.50]
Fe	0.13 [0.05–0.23]	0.19 [0.10–0.32]
Flux[c]	4.3e-12	5.0e-12
L_X[d]	7.4e+32	8.6e+32

Notes.
[a] Confidence intervals are given in brackets, and all abundances are expressed as ratios to their solar values. See Section 3.2.2.
[b] Emission measure in units of cm^{-3}.
[c] Intrinsic (unabsorbed, $N_H = 0$) X-ray fluxes in units of erg cm^{-2} s^{-1}.
[d] Intrinsic X-ray luminosity ($D = 1.2$ kpc) in units of erg s^{-1}.

with the typical visual (dust) extinction measured toward the regions of the nebula from which X-rays are detected ($A_V \sim 1$–2; Kastner et al. 2002). Adopting the (overly simplistic) assumption that the absorption arises in a spherically symmetric envelope surrounding the X-ray emitting plasma, the best-fit value of N_H in the two-component model implies a neutral envelope mass of $\sim$0.03 $M_\odot$—in reasonable agreement with available estimates (e.g., Bachiller et al. 1991). We conclude that N_H is unlikely to be overestimated due to the assumption of solar abundances in the absorbing column (implicit via use of the `wabs` model).

In addition, the confidence contour plots demonstrate that the C and Ne abundance parameters are well correlated with O, indicating that the C/O and Ne/O ratios (as well as other key abundance ratios, such as Fe/O) are very well constrained by the LETG spectrum (Figure 7), even though the individual absolute abundances remain uncertain, due to the lack of constraints on the plasma H abundance. Specifically, we find C/O $\sim$ 15–45, Ne/O $\sim$ 3.3–5, N/O $\sim$ 0–1.0, and Fe/O $\sim$ 0.1–0.4, relative to the solar ratios. The existence of a large C overabundance (relative to solar) is supported by the tight constraints placed on N_H and the lack of correlation between inferred C abundance and N_H (Figure 6). That is, it is unlikely that the inferred high C abundance can be attributed to an overestimate of the intervening absorption due to neutral metals. However, as just discussed, it is also unlikely that the abundance of C has been vastly underestimated due to the assumption of standard (solar) metal abundances in the absorbing material. Figure 8, furthermore, makes clear that the inferred C, O, and Ne abundances are relatively insensitive to the best-fit plasma temperatures.

4. DISCUSSION

4.1. Plasma Modeling: Comparison with Previous Results

In Table 4, we compare previous results from X-ray CCD spectroscopy of BD +30°3639 with those obtained from modeling its LETG/ACIS spectrum (Section 3.2). Whereas the value of T_X obtained from the isothermal model (Table 3) is on the low side of the range found in the CCD-based work—likely reflecting the spectral dominance of the longer-wavelength lines of C and O—the temperatures determined from the two-component model fit bracket the range of values previously determined from CCD spectra. Although the LETG-S modeling definitively demonstrates that isothermal models are not adequate to match the line spectrum in detail (Section 3.2.1), the comparison to previous work, as well as to the isothermal model explored here, suggests that single-component plasma models that are based on X-ray CCD spectra are capable of recovering the characteristic temperature (as opposed to the temperature extremes) of the superheated plasma in PNs.

The LETG/ACIS spectral modeling confirms the Ne and C enrichment and Fe underabundance in the X-ray emitting plasma of BD +30°3639 that were previously inferred from X-ray CCD spectra, albeit with much improved constraints on the degree of these abundance anomalies (relative to O). In particular, the LETG/ACIS spectral modeling—while confirming that C is highly enriched in the X-ray emitting plasma—definitively precludes a plasma C/O ratio larger than $\sim$45, relative to solar. Indeed, our lower limit on the C/O ratio in the diffuse X-ray emission (C/O $\sim$15) is much more consistent with the ratio at the central star, as derived from optical/UV spectroscopy (C/O $\sim$12; Leuenhagen et al. 1996; Marcolino et al. 2007), than with the ratio characteristic of the nebular gas (C/O $\sim$1.6; Pwa et al. 1986).

In contrast to the case of C, whose large overabundance is evident from the strength of the resonance line of C VI, there is no unambiguous evidence for Fe emission lines in the entire LETG/ACIS spectrum of BD +30°3639. Although a line is present at $\sim$15.15 Å that may be partly due to 15.014 Å line emission from Fe XVII, it is likely that the O VIII line at 15.1670 Å contributes to (or even dominates) the flux measured for the $\sim$15.15 Å line. In addition, we do not clearly detect any Fe XVII emission lines around 17 Å; these lines are expected to be bright at the relatively low plasma temperatures found here (Doron & Behar 2002). Furthermore, there is no evidence for lines of Fe XVI (or Fe XVIII), such as might be expected if the temperature were too low (or too high) for efficient formation of Fe XVII via ionization equilibrium. This lack of Fe lines results in a firm upper limit on an Fe abundance of $\sim$0.3 relative to solar (Table 3), consistent with the optical/UV results of Georgiev et al. (2006)

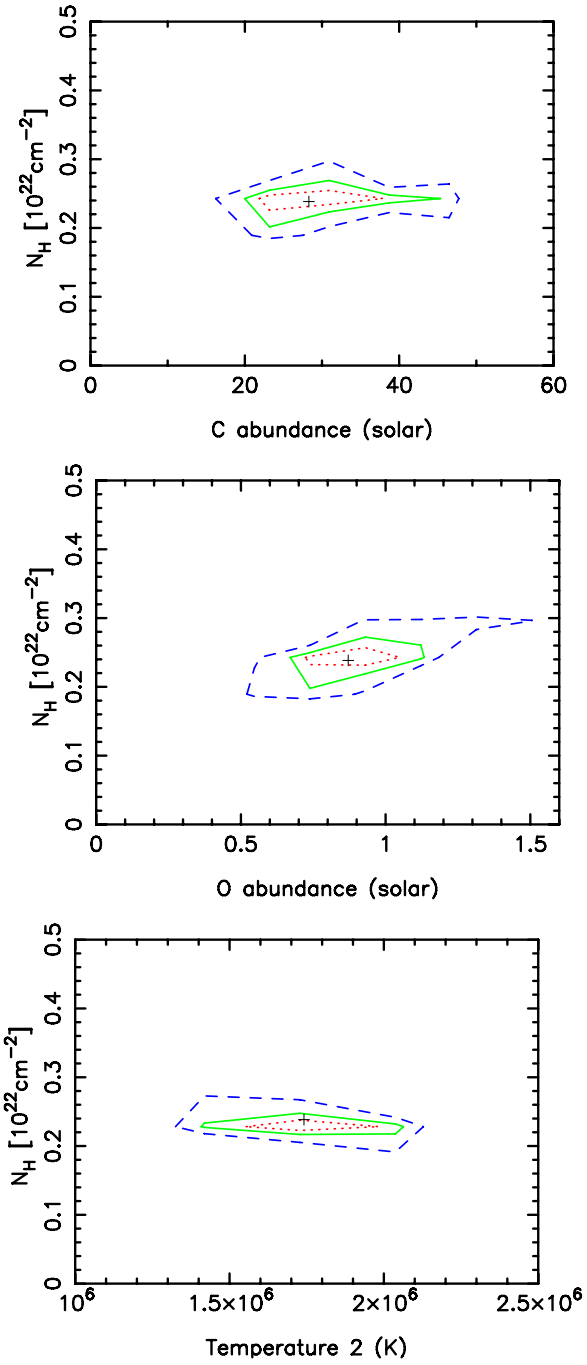

Figure 6. Plots of best-fit confidence contours (68%, dotted; 90%, solid; and 99%, dashed), as obtained from the two-component APED model fitting, for the column density parameter $N_{\rm H}$ vs. the C abundance parameter (top), O abundance parameter (middle), and the lower of the two temperatures (bottom).

(A color version of this figure is available in the online journal.)

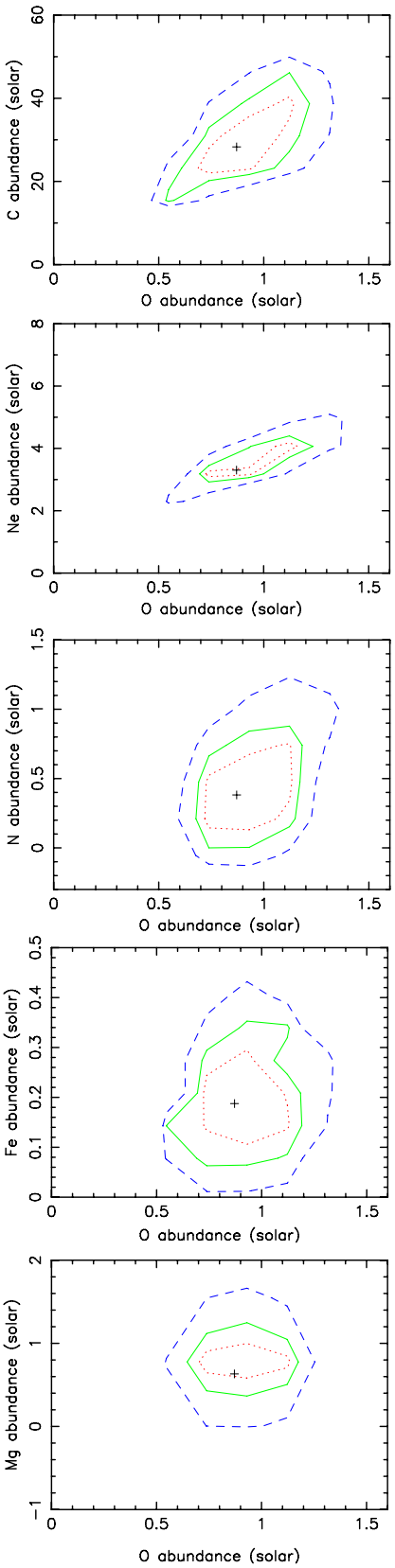

Figure 7. As in Figure 6 for the C, Ne, N, Fe, and Mg abundance parameters (top to bottom, respectively) vs. the O abundance parameter.

(A color version of this figure is available in the online journal.)

for the nebula and Marcolino et al. (2007) for the central star.

In addition, the 24.8 Å resonance line of N VII is not detected, although the line flux is not as well constrained as that of Fe XVII due to the low sensitivity of LETG/ACIS in the former wavelength regime. As a consequence of this nondetection, the N abundance obtained from the LETG/ACIS spectral modeling demonstrates that N is, if anything, underabundant relative to solar, contradicting several previous X-ray abundance studies. Our gratings-based result of an N underabundance, which is consistent with optical/UV results for the central star (Marcolino et al. 2007), indicates that modeling of previous (CCD) X-ray spectra has confused N with C. We also find that

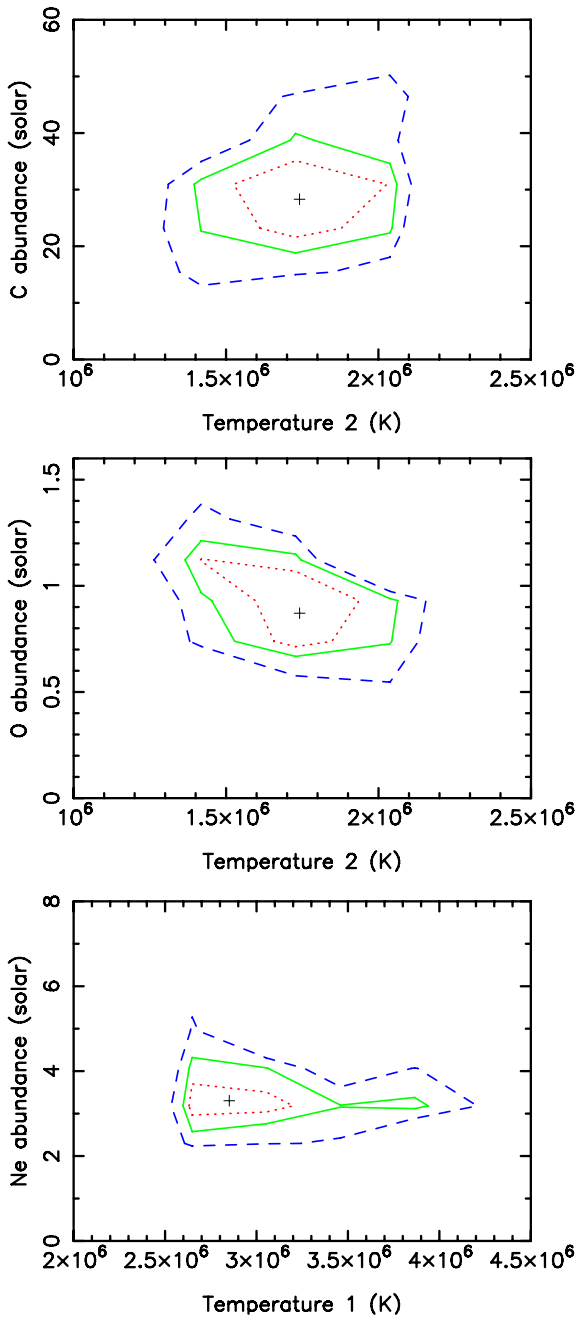

Figure 8. As in Figure 6 for C and O abundances vs. the lower of the two temperatures (top and middle panels) and the Ne abundance vs. the higher of the two temperatures (bottom).

(A color version of this figure is available in the online journal.)

previous indications of depleted Mg obtained from CCD spectra are not supported by the LETG data.

The absorbing column and (thus) intrinsic X-ray luminosity inferred from the LETG/ACIS modeling are on the high side of the range of values previously determined from X-ray CCD spectra (Table 4). However, the LETG spectral modeling has significantly decreased the uncertainty in the inferred values of $N_{\rm H}$ and, hence, L_X.

4.2. Plasma Abundances: Constraints on the Origin of the X-Ray Emitting Gas

The similarity of the large overabundance of C and underabundance of Fe that we determine from the LETG/ACIS spectral modeling to these same anomalies as determined for the central star (Marcolino et al. 2007, and references therein) traces the X-ray emitting gas directly back to the present-day central star. Indeed, the mass fractions one would deduce from Table 3 under the assumption that the C/He number ratio is identical to that of the central [WC] star—41.5% for He, 49.7% C, 4.8% O, 3.3% Ne, less than 0.24% N, and less than 0.2% Fe—agree remarkably well with those found by Marcolino et al. (2007) for the [WC] stellar wind. Furthermore, our robust determination of an Ne overabundance of ∼3 to ∼6 relative to solar is consistent with the predictions of models describing H-deficient central stars of PNs (Werner & Herwig 2006). Hence, as also pointed out by Murashima et al. (2006) and Kastner et al. (2006), the nonsolar composition of the X-ray emitting plasma in BD +30°3639 appears to be the direct result of nucleosynthesis processes in the precursor AGB star (e.g., Herwig 2005, and references therein).

These results indicate that the shocked plasma now seen in X-rays originated deep within the AGB star, in the "intershell" region; He-shell burning just below this region is responsible for the generation of C. Meanwhile, the observed enhanced Ne/O and low Fe/O, N/O, and Mg/O abundance ratios can be explained as a natural consequence of the s-process within the "pulse-driven convection zone" (Herwig 2005). The Ne may predominantly be ^{22}Ne, which can be readily generated—at the expense of ^{14}N—within the He burning shell. The ^{22}Ne can then serve as an iron-depleting neutron source during the s-process. In such a scenario, one therefore expects Ne to be enhanced, while Fe, N, and Mg are depleted relative to O, as observed (Table 3).

4.3. The Temperature of X-Ray Emitting Plasma within BD +30°3639

The two plasma temperatures obtained from our best-fit, two-component APED model—1.7 × 10^6 K and 2.9 × 10^6 K—likely represent the extremes of a continuous range of temperature within BD +30°3639. Hence, the spectral diagnostics available in the LETG/ACIS X-ray spectrum of BD +30°3639 conclusively demonstrate, for the first time, the presence of a temperature gradient within the X-ray emitting region of a PN. However, even the higher of these two temperatures, obtained from those line ratios that are diagnostics of the hottest plasma present in the LETG/ACIS-S first-order spectrum, is far lower than that expected from simple adiabatic shock models, given the present-day central star fast wind speed (700 km s^{-1}; Leuenhagen et al. 1996; Marcolino et al. 2007). This discrepancy between observed and predicted hot bubble plasma temperatures has been noted by many investigators over the past decade (e.g., Arnaud et al. 1996; Chu et al. 2001; Soker & Kastner 2003, and references therein), and was recently discussed by Kastner et al. (2008) in their analysis of the collective *Chandra* and *XMM-Newton* data compiled to date for PN hot bubbles. The temperature discrepancy has been previously explained as indicative of heat conduction from the tenuous hot bubble to the dense, relatively cool, swept-up shell (Stute & Sahai 2007; Schönberner et al. 2006; Steffen et al. 2008) or mixing of the two media (Chu et al 1997; Stute & Sahai 2006).

However, such models of mixing and heat conduction predict that the bulk of the X-ray emission arises in the same gas that is responsible for the visible-light nebula (Steffen et al. 2008). Our robust determination of nonsolar abundances (in particular, greatly enhanced C and Ne) in the X-ray emitting

Table 4
BD +30°3639: Comparison of LETG and X-ray CCD Spectrum Plasma Model Fitting Results

Parameter	A96 *ASCA*/*SIS*	K00	M03 *Chandra*/ACIS-S3	G06	M06 Suzaku/XIS	This Paper *Chandra*/LETG/ACIS
N_H (10^{22} cm^{-2})	0.12	0.1 [0.09–0.11]	0.24 [0.23–0.25]	0.2 [1.7–2.3]	0.21[1.4–2.5]	0.24 [0.20–0.28]
L_X (10^{32} ergs s^{-1})	1.3–1.7	2.3	...	...	12	8.6
T_1 (10^6 K)	3.0 [2.7–3.3]	2.7 [2.6–2.8]	2.1 [2.08–2.12]	2.4 [2.1–2.6]	2.2 [2.1–2.3]	2.9 [2.6–3.3]
T_2 (10^6 K)	...	...	...	...	...	1.7 [1.3–2.1]
Fe/O	0	...	0	0.3 [0.1–0.8]	<0.1	0.2 [0.1–0.4]
Ne/O	8.3	...	4.6 [3.9–5.3]	5.4 [0.1–57.7]	5.8 [4.7–7.5]	3.8 [3.3–5.0]
C/O	281	...	84 [79–90]	97 [8.1–813]	85 [71–101]	32.5 [15–45]
N/O	7.2	...	2.2 [2.0–2.3]	5.8 [1.3–80.1]	3.2 [0.9–5.5]	0.4 [0.0–1.0]
Mg/O	...	...	0.24 [0.22–0.26]	0.3 [0.1–0.8]	...	0.7 [0.4–1.5]

Notes.
90% confidence intervals are given in brackets, and all abundance ratios are expressed as relative to their solar values. Intrinsic luminosity (L_X) is calculated on the basis of $D = 1.2$ kpc.
References. A96 = Arnaud et al. 1996; K00 = Kastner et al. 2000; M03 = Maness et al. 2003; G06 = Georgiev et al. 2006; M06 = Murashima et al. 2006.

plasma within BD +30°3639 therefore indicates that the shocked gas is predominantly the present-day stellar wind or jet, as opposed to nebular gas. Hence, the heat conduction and mixing mechanisms, though certainly viable in the general case, do not play a major role in determining the X-ray temperature of this particular PN. We note that this argument likely holds even at early stages of the heat conduction process. This is because at early times, the conduction goes through the "evaporation" stage, where the intermediate-temperature gas comes from the cold phase (Borkowski et al. 1990). In PNs, the cold phase is the visible nebular gas, and the abundance results obtained here preclude such an origin for the X-ray emitting plasma.

There remains the possibility that the shocked wind presently seen in X-rays was ejected at an earlier epoch when the fast wind speed was ∼ 300–400 km s^{-1}, a velocity regime more consistent with the measured range of T_X (Arnaud et al. 1996; Akashi et al. 2006, 2007). Alternatively, collimated jets, perhaps associated with molecular "bullets" detected in mm-wave interferometric imaging (Bachiller et al. 2000), may be responsible for the X-ray emission. Such a scenario would be similar to that proposed for NGC 7027 (Kastner et al. 2002; Cox et al. 2002) and would be consistent with the possibility that BD +30°3639 is a bipolar nebula viewed nearly pole-on (Kastner et al. 2002; Lee & Kwok 2005). This possibility will be pursued in our forthcoming paper concerned with spatial analysis of the LETG/ACIS data (Y. S. Yu et al. 2008, in preparation).

5. CONCLUSIONS

Using *Chandra*'s LETG/ACIS-S spectrometer, we have obtained the first X-ray gratings spectrum of a PN. The LETG/ACIS-S spectrum of the young, rapidly evolving BD +30°3639 displays strong emission in the H-like resonance lines of O VIII and C VI and He-like triplet line complexes of Ne IX and O VII, and appears devoid of lines of highly ionized Fe and N. Our spectral modeling, consisting of fits of variable-abundance APED plasma models with one and two temperature components, demonstrates that an isothermal plasma is unable to simultaneously reproduce key spectral features, such as the O VII to O VIII and Ne IX to Ne X line ratios and the 6–18 Å continuum. The best-fit two-component plasma model, which is able to well match these same features, indicates that the X-ray emission line spectrum is representative of a range of temperatures from ∼1.7 MK to ∼2.9 MK. These results constitute the first case in which a temperature gradient has been inferred within the X-ray emitting region of a PN.

The spectral modeling places tight constraints on the degree of abundance anomalies present in the X-ray emitting plasma within BD +30°3639, convincingly demonstrating that Fe is highly deficient (best-fit Fe/O ∼0.3, relative to the solar ratio) and that C and Ne are highly enhanced in abundance (best-fit ratios C/O ∼30 and Ne/O ∼4). This C overabundance, although very large, is not as pronounced as previously deduced on the basis of X-ray CCD spectroscopy. In addition, based on the LETG/ACIS-S line spectrum, we find no evidence for enhanced N and depleted Mg, as previously inferred from CCD spectra; indeed, if anything, N is somewhat underabundant in the X-ray emitting gas.

The sharply nonsolar composition of the X-ray emitting plasma is similar to that determined for the present-day central star of BD +30°3639 via optical/UV spectroscopy. We conclude that the plasma predominantly consists of very recently ejected gas originating from nucleosynthesis processes that occurred deep within the progenitor AGB star. The "pristine" state of this C- and Ne-enriched (and Fe-depleted) plasma suggests that processes such as heat conduction and/or mixing between the superheated plasma and cooler, denser nebular gas may not suffice to explain the fact that the inferred range of X-ray emission temperatures is well below that expected for shocks generated by the present-day, 700 km s^{-1} central star wind. Instead, it appears that the shocks detected via X-rays likely result from lower-speed (300–400 km s^{-1}) ejections, perhaps in the form of collimated jets and/or reflecting the rapid evolution of the central star wind.

The intrinsic X-ray luminosity we deduce from the modeling, $\sim 10^{33}$ erg s^{-1}, is approximately an order of magnitude larger than some previous CCD-based estimates. This luminosity lies at the very highest end of the range of L_X predicted by models describing either spherically symmetric PN hot bubbles or pulsed jets in symbiotic stars (e.g., Stute & Sahai 2006, 2007), suggesting that the wind collisions in BD +30°3639 are indeed very strong. Such strong wind interactions may, however, be commonplace in PN with [WC] central stars (K08). In these and other respects, the plasma abundances, temperatures, and luminosity determined from the dispersed X-ray spectrum of BD +30°3639 should serve both to constrain models of stellar evolution and to guide the development of sophisticated models

of the wind interactions responsible for the superheated gas within PNs.

This research was supported by NASA through *Chandra* award GO5-6008X issued to Rochester Institute of Technology by the *Chandra X-Ray Observatory Center*, which is operated by Smithsonian Astrophysical Observatory for and on behalf of NASA under contract NAS8-03060.

REFERENCES

Akashi, M., Soker, N., & Behar, E. 2006, MNRAS, 368, 1706
Akashi, M., Soker, N., Behar, E., & Blondin, J. 2007, MNRAS, 375, 137
Akashi, M., Meiron, Y., & Soker, N. 2008, in press, arXiv:0711.3265
Anders, E., & Grevesse, N. 1989, Geochim. Cosmochim. Acta, 53, 197
Arnaud, K., Borkowski, K. J., & Harrington, J. P. 1996, ApJ, 462, L75
Bachiller, R., Forveille, T., Huggins, P. J., Cox, P., & Maillard, J. P. 2000, A&A, 353, L5
Bachiller, R., Huggins, P. J., Cox, P., & Forveille, T. 1991, A&A, 247, 525
Borkowski, K. J., Balbus, S. A., & Fristrom, C. C. 1990, ApJ, 355, 501
Cash, W. 1979, ApJ, 228, 939
Chu, Y.-H., Chang, T. H., & Conway, G. M. 1997, ApJ, 482, 891
Chu, Y.-H., Guerrero, M. A., Gruendl, R. A., Williams, R. M., & Kaler, J. B. 2001, ApJ, 553, L69
Chu, Y.-H., Kwitter, K., & Kaler, J. B. 1993, AJ, 106, 650
Cox, P., Huggins, P. J., Maillard, J.-P., Habart, E., Morisset, C., Bachiller, R., & Forveille, T. 2002, A&A, 384, 603
Dewey, D. 2002, in Proc. High-Resolution X-ray Spectroscopy with XMM-Newton and Chandra, ed. G. Branduardi-Raymont (London: Univ. College London), http://www.mssl.ucl.ac.uk/_gbr/rgs_workshop/
Doron, R., & Behar, E. 2002, ApJ, 574, 518
Georgiev, L. N., Richer, M. G., Arrieta, A., & Zhekov, S. A. 2006, ApJ, 639, 185
Guerrero, M. A., Chu, Y.-H., & Gruendl, R. A. 2000, ApJS, 129, 295
Herwig, F. 2005, ARA&A, 43, 435
Houck, J. C., & Denicola, L. A. 2000, ASPC, 216, 591
Kastner, J. H., Li, J., Vrtilek, S. D., Gately, I., Merrill, K. M., & Soker, N. 2002, ApJ, 581, 1225
Kastner, J. H., Montez, R., Balick, B., & De Marco, O. 2008, ApJ, 672, 957
Kastner, J. H., Soker, N., Vrtilek, S. D., & Dgani, R. 2000, ApJ, 545, L57
Kastner, J. H., Vrtilek, S. D., & Soker, N. 2001, ApJ, 550, L189
Kastner, J. H., Yu, Y. S., Houck, J., Behar, E., Nordon, R., & Soker, N. 2006, in IAU Symp. 234, Planetary Nebulae in Our Galaxy and Beyond, ed. M. J. Barlow & R. H. Mendez (Cambridge: Cambridge Univ. Press), 169
Kreysing, H. C., Diesch, C., Zweigle, J., Staubert, R., Grewing, M., & Hasinger, G. 1992, A&A, 264, 623
Kwok, S., Purton, C. R., & Fitzgerald, P. M. 1978, ApJ, 219, L125
Lee, T.-H., & Kwok, S. 2005, ApJ, 632, 340
Leuenhagen, U., Hamann, W. R., & Jeffery, C. S. 1996, A&A, 312, 167
Li, J., Harrington, J. P., & Borkowski, K. 2002, AJ, 123, 2676
Maness, H. L., Vrtilek, S. D., Kastner, J. H., & Soker, N. 2003, ApJ, 589, 439
Marcolino, W. L. F., Hillier, D. J., de Araujo, F. X., & Pereira, C. B. 2007, ApJ, 654, 1068
Morrison, R., & McCammon, D. 1983, ApJ, 270, 119
Murashima, M., et al. 2006, ApJ, 647, L131
Pwa, T. H., Pottasch, S. R., & Mo, J. E. 1986, A&A, 164, 184
Schönberner, D., Steffen, M., & Warmuth, A. 2006, in IAU Symp. 234, Planetary Nebulae in Our Galaxy and Beyond, ed. M. J. Barlow & R. H. Mendez (Cambridge: Cambridge Univ. Press), 161
Soker, N. 1994, MNRAS, 270, 774
Soker, N., & Kastner, J. H. 2003, ApJ, 583, 368
Smith, R. K., Brickhouse, N. S., Liedahl, D. A., & Raymond, J. C. 2001, ApJ, 556, L91
Steffen, M., Schönberner, D., Warmuth, A., Schwope, A., Landi, E., Perinotto, M., & Bucciantini, N. 2005, in AIP Conf. Proc. 804, Planetary Nebulae as Astronomical Tools, ed. R. Szczerba, G. Stasińska, & S. K. Gorny (New York: Melville), 161
Steffen, M., Schönberner, D., & Warmuth, A. 2008, A&A, 489, 173S
Stute, M., & Sahai, R. 2006, ApJ, 651, 882
Stute, M., & Sahai, R. 2007, ApJ, 665, 698
Werner, K., & Herwig, F. 2006, PASP, 118, 183
Zhekov, S. A., & Perinotto, M. 1996, A&A, 309, 648
Zhekov, S. A., & Myasnikov, A. V. 1998, NewA, 3, 57
Zhekov, S. A., & Myasnikov, A. V. 2000, ApJ, 543, L53